

A single transmitter multi-receiver (STMR) PZT array for guided ultrasonic wave based structural health monitoring of large isotropic plate structures

Jagannathan Rajagopalan, Krishnan Balasubramaniam and C V Krishnamurthy

Center for Nondestructive Evaluation and Department of Mechanical Engineering,
Indian Institute of Technology, Madras, Chennai-600036, India

E-mail: balas@iitm.ac.in

Received 22 February 2005, in final form 27 April 2006

Published 21 July 2006

Online at stacks.iop.org/SMS/15/1190

Abstract

A new compact sensor configuration comprising a single transmitter and multi-receivers (STMR) is presented for the *in situ* structural health monitoring (SHM) of large plate-like isotropic structures. The STMR exploits the long-range propagation characteristics of ultrasonic guided Lamb waves and a phase reconstruction algorithm to provide defect detection and location capability under non-dispersive as well as dispersive regimes of guided waves. Simulations are performed on defect-free and defective finite plates of aluminum to demonstrate the various features of the STMR system. Experiments were carried out on 1 mm thick aluminum plates initially using a pair of individual sensors and subsequently using a prototype STMR array. The simulated results of the STMR performance were validated well through these experiments. Features of the STMR system such as its small footprint, the relatively simple data acquisition and processing discussed here have applications in the SHM of plate-like structures, and particularly of aerospace structures.

(Some figures in this article are in colour only in the electronic version)

1. Introduction

Structural health monitoring (SHM) is one of the aspects of a smart structure, and it can be defined as the acquisition and analysis of technical data to facilitate life cycle management decisions. It denotes an 'intelligent' system, which is able to detect and interpret adverse changes in the structure, which will greatly reduce the life cycle cost. Some of the advantages of SHM over conventional non-destructive evaluation (NDE) inspection would be reduced inspection downtime, elimination of component tear down, and potential prevention of failure during operation. This could well be used in identifying failures in aircraft, which would be a boon to the aircraft industry, which reportedly spends 27% of the life cycle cost on inspection [1].

Thin plate-like structures find a variety of applications in the aerospace industry, wing panels being one of them. Inspection of these structures using conventional NDE techniques like C-scans is very time-consuming. Guided waves, particularly Lamb waves, use the bounding surfaces of a plate to propagate long distances and are therefore attractive for inspection of large area structures especially in terms of the time consumed for inspection [2, 3]. Although Lamb waves are dispersive and multi-moded [4], several attempts have been made exploiting synthetic array techniques to increase the signal to noise ratio, to achieve beam steering, and to compensate for dispersion effects [5–9]. It has been shown that the use of multiple transducers in a phased manner provides improved transduction and increases the area of coverage [10]. Structural health monitoring of isotropic

and anisotropic plate-like structures by processing data from multi-transmitters and multi-receivers, made of PZT crystals, using tomographic reconstruction techniques has been reported elsewhere [11, 12]. The applicability of an electromagnetic acoustic transducer (EMAT) array based system, consisting of multi-transmitters and multi-receivers, for rapid inspection of plate structures using a beam steering algorithm (that has many similarities to the phase reconstruction algorithm discussed in this paper) has been demonstrated in [13]. Techniques based on beam forming using ‘phased arrays’ and time-reversal concepts are demonstrated for example in [14] and [15] respectively.

In this paper, we demonstrate the use of an SHM system comprising a single transmitter and a circular array of receivers for monitoring the health of large isotropic plate-like structures. Unlike traditional NDE techniques, the SHM technique is expected to provide a continuous damage monitoring capability

- (a) in an *in situ* monitoring mode, using a long range guided wave approach
- (b) at less cost, due to reduced downtime for routine inspection
- (c) that was not previously possible, due to increased sensitivity
- (d) with increased reliability, using multi-mode approach
- (e) where accessibility for performing inspection was previously limited, due to guided nature of the wave modes and, most importantly,
- (f) provide an early warning methodology for in-service damage detection so that appropriate corrective action can be undertaken.

In sections 2 and 3 of the paper, we describe the array system and the method of data acquisition. In section 4, we describe the data processing method, which utilizes a phased addition algorithm in the wavenumber domain, which locates any structural features or defects present in the structure. In sections 5 and 6, we present the results from simulations and experiments and discuss the capabilities of the system.

2. STMR array description

The STMR array consists of a single transmitter and N receivers that are acoustically coupled to one surface of the plate. The receivers are arranged in a circle of diameter D while the transmitter is placed at its center. A prototype STMR array, with a transmitter (indicated as T) and 15 receivers (indicated as R) located at 15 equi-spaced points on circle of 15 cm diameter is shown in figure 1. The array configuration, described in greater detail elsewhere [5], consists of a single transmitter to ensure uniform coverage and avoid non-uniform insonification associated with beam formation reported for the multi-transmitter multi-receiver (MTMR) system [10]. It also simplifies the task of data collection considerably as only the receivers are to be ‘arrayed’. The circumferential arrangement of the receivers enables the received ‘beam’ (after phased addition) to be steered in any direction, thereby achieving omni-directionality in performance. To achieve high angular resolution in the reconstructed image, the steering and hence the reconstruction needs to be carried out for a large number of angles. The parameters governing the image reconstruction

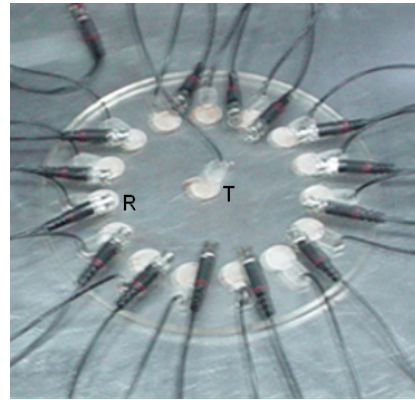


Figure 1. A prototype of the STMR PZT array used in the experiments.

(This figure is in colour only in the electronic version)

therefore are the diameter of the circular array, D , the number of receivers, N , and the number of reconstruction angles, n . For carrying out simulations, the transmitter and the receivers are assumed to act as point sources and are considered to have equal transmission and reception sensitivity in all directions. Experiments were carried out with conventional PZT crystals and the simulated results were well validated, justifying the point source/receiver assumption made in the simulations.

3. Data acquisition and transformation

The acquisition of the raw data set in the time, t , domain, in digital format, represents the Lamb wave data set. The transmitter is excited and a discretely sampled t domain signal is collected at each of the receivers. These data are arranged to form a matrix, \mathbf{T} , in which each column represents the raw t domain signal collected at each of the N receivers. When the wave propagation is non-dispersive the phase velocity is constant and the time domain data can be directly transformed to spatial domain data enabling flaw location and sizing through phased addition procedures. Under dispersive conditions, the phase velocity is not a constant and the relation $k = \omega/v_{ph}$ (where v_{ph} is the phase velocity) leads to non-uniformly spaced wavenumber domain data that are unsuitable for carrying out phased addition procedures for locating and sizing the flaw. To compensate for the guided wave dispersion [16], each column in the \mathbf{T} matrix is fast Fourier transformed to yield a matrix \mathbf{F} containing the complex spectra at equi-spaced points in the frequency, ω , domain. Then, the frequency domain data in \mathbf{F} are transformed to wavenumber domain data using a linear interpolation scheme [10] resulting in a matrix, \mathbf{W} , of equi-spaced data in the wavenumber domain. The rows in \mathbf{W} are referred to by the subscript i and the corresponding wavenumber is k_i . It is important to note that the number of rows and columns in \mathbf{W} is equal to those in \mathbf{F} . The entire procedure is summed up in figure 2.

4. Algorithm for phase reconstruction

The purpose of the phase reconstruction algorithm is to determine the locations from which the waves sent by the

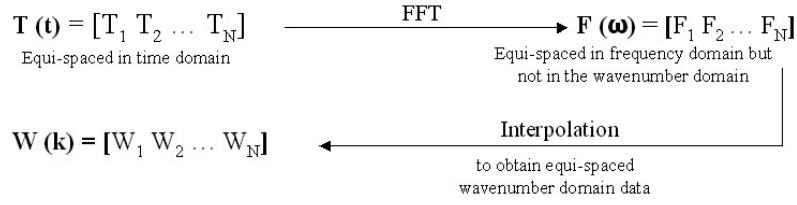


Figure 2. Schematic representation of the transformation of data from time (t) domain to wavenumber (k) domain.

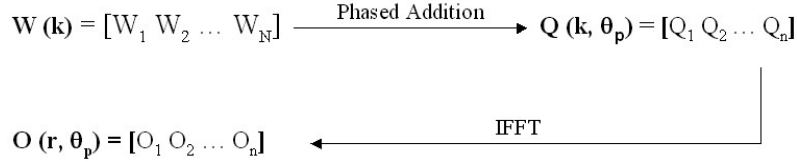


Figure 3. Schematic of the phase reconstruction procedure.

transmitter are reflected back. In the algorithm, the reflected wavepackets are assumed to come from a particular direction (angle) and the signal received at each receiver is shifted appropriately (in the k domain) and added. If the assumed direction is the actual direction of the reflected wave then this process results in a coherent addition. This procedure is repeated for a set of equi-spaced angles that span the entire 360° . The locations from which the waves are reflected back are then obtained by performing an inverse fast Fourier transform (IFFT) on these phase-reconstructed signals.

In the first step of the algorithm, a particular guided wave mode is chosen and phased addition of the columns of \mathbf{W} matrix is performed along n equi-spaced reconstruction angles using the dispersion characteristics of the mode. These reconstruction angles, represented by θ_p , are the assumed angles of propagation of the reflected waves. This phased addition in the k domain leads to a matrix, \mathbf{Q} , in which the rows represent different wavenumbers, k_i , and the columns represent different reconstruction angles, θ_p . The elements in \mathbf{Q} are calculated using the following expression.

$$q_{ip} = \sum_{j=1}^N w_{ij} \exp(-i2\pi k_i x_{pj}) \quad (1)$$

where,

$$x_{pj} = r_j \cos(\Phi_j - \theta_p). \quad (2)$$

In the above expressions r_j and Φ_j are the polar coordinates of the j th receiver, while x_{pj} represents the change in path length required for the signal received by the j th receiver to maintain coherence along θ_p . To obtain the output matrix, \mathbf{O} , in the polar domain, the columns in \mathbf{Q} are subject to an inverse fast Fourier transform (IFFT) to convert them from the k domain to the r domain. Now each row in \mathbf{O} corresponds to a particular radius while each column corresponds to a particular angle. It is important to note that the number of columns in \mathbf{Q} and \mathbf{O} is equal to n , the number of reconstruction angles used. Reconstruction is obtained by plotting the amplitudes of the elements in \mathbf{O} as a function of their polar position. The algorithm for the reconstruction is summed up in figure 3.

The phase correction algorithm effectively approximates the path lengths between the flaw and the receiver to be equal to

the projection along the angle that is being reconstructed [6, 7]. In other words, the algorithm requires the flaw to be in the far-field of the receiver array. The algorithm also ignores signal strength reduction due to material attenuation and beam spreading. Noting that the actual receiver positions on the circle get projected onto a diameter during the reconstruction process, the angular resolution achievable for the reconstruction can be seen to be proportional to λ/D , and the near-field to far-field transition to be proportional to D^2/λ , where λ denotes the wavelength of the mode under consideration. These two opposing trends help limit the footprint of the STMR system to be small enough and yet be attractive in practical applications.

5. Simulation studies

The scope of the STMR system is brought out through simulations subsequently validated through in-house experiments with realistic parameters. An STMR system, consisting of a transmitter at the centre and 30 receivers placed on the circumference of a circle of 8 cm diameter, was considered, placed on a 1 mm thick Al plate with infinite planar dimensions. The dispersion curves for Al at low frequencies indicate the presence of two modes, S_0 and A_0 , with S_0 being the faster mode. We chose the S_0 mode, the dispersion characteristics of which are shown in figure 4(a), for excitation in the simulations. Figures 4(b) and (c) show the RF signal wave forms for excitations at the nearly non-dispersive region (0.5 MHz mm) and fairly dispersive region (2 MHz mm) of the S_0 mode.

As a first case, the response from a single point reflector located in the $\theta = 180^\circ$ direction at a distance of 50 cm from the array center, taken to be in the far-field of the STMR array, is considered. Using the position of the defect with respect to each receiver, the total distance traveled by the wave to reach each receiver was calculated. Then, the dispersion characteristics of the guided wave mode of interest were used to shift each component in the transmitted signal appropriately in the time domain. The time-shifted components were added to get the time domain signal at each of the receivers yielding the \mathbf{T} matrix. Further processing was done using the procedure

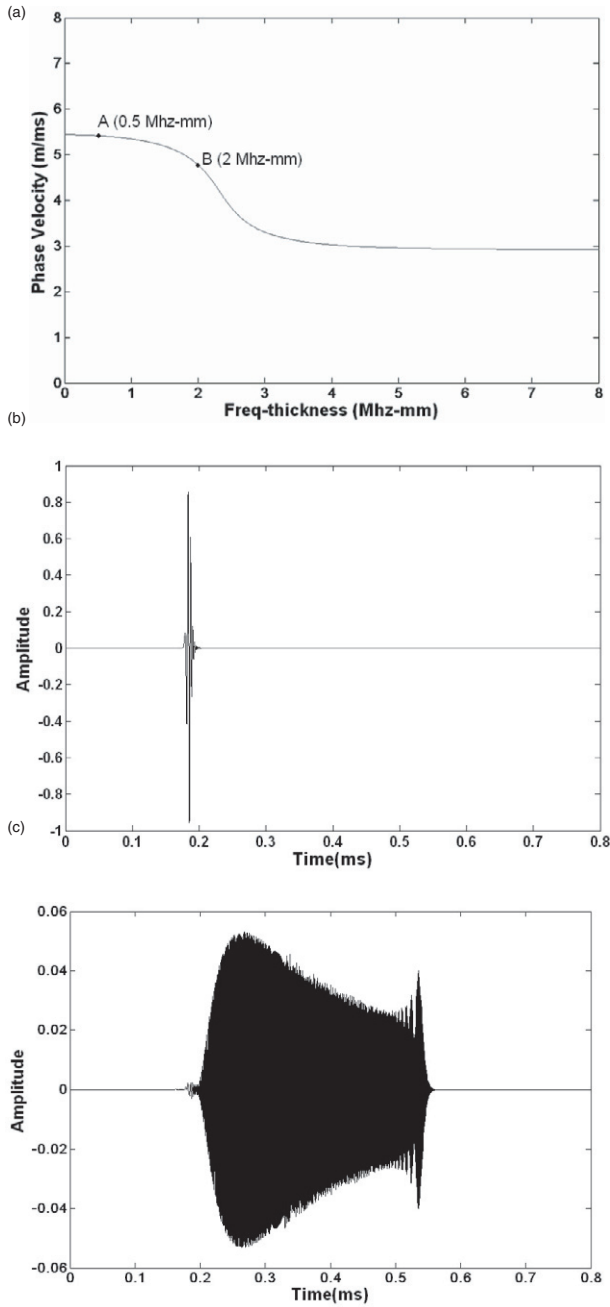


Figure 4. (a) Dispersion curve of the S_0 mode in 1 mm thick Al plate. Points A and B have been chosen to indicate the effect of ignoring dispersion effects during image reconstruction. (b) Reflected signal from a defect placed at 50 cm along the 180° line: simulation at 0.5 MHz where the dispersion effects of the S_0 mode are barely visible. (c) Reflected signal from a defect placed at 50 cm along the 180° line: simulation at 2 MHz where the dispersion effects of the S_0 mode are significant.

outlined in the above sections. The image of the defect reconstructed including the dispersion effects is shown in figure 5(a). The grayscale on the plot is logarithmic with a range of 12 dB. Although a 6 dB scale is adequate when dealing with strong reflections, the 12 dB scale was chosen to allow for weak scattering events as well. The position of the array and the defect are indicated in the figure. The defect can be seen at

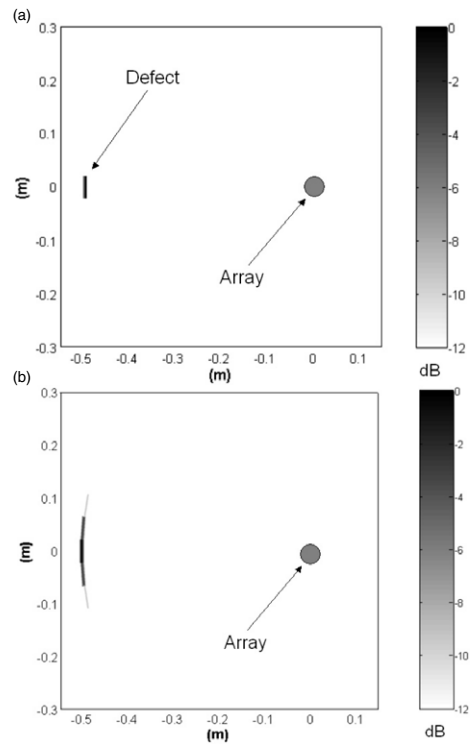


Figure 5. (a) Reconstruction, including dispersion, of a simulated defect 50 cm from the array center located along the 180° direction: excitation pulse at 0.5 MHz frequency. (b) Reconstruction of the case shown in figure 5(a), but ignoring dispersion.

the assumed defect location as a black patch. The black patch indicates higher amplitude, which has been obtained as a result of the coherent addition of the reflected signals obtained at the various receivers.

The need for considering mode dispersion can be judged from comparing figure 5(a) with 5(b), obtained by deliberately ignoring dispersion effects in the algorithm. Dispersion effects, though weak at this frequency, are seen to cause considerable broadening of the defect signature. Figures 6(a) and 6(b), which show a large number of artifacts and considerable blurring of the defect signature, are the reconstructed images with and without considering dispersion effects at 2 MHz. It can be seen from these examples that the algorithm can handle dispersive effects effectively. Although wavenumber interpolation is not required in the absence of dispersion, the algorithm has been written to handle dispersion-free situations in a natural manner.

The performance of the algorithm in the case of multiple flaws has been examined through another simulation, with three defects assumed to be along $\theta = 90^\circ$, 180° and 270° respectively. The results of this simulation are shown in figure 7, where the defects can be seen as black patches at the assumed defect locations.

Partially mode converted signals, due to flaw scattering, pose no difficulties in reconstruction. In the cases where the reflected signals have unknown mode components, the algorithm can be made to sift through various modes during the analysis of the reflected signals and the reconstruction can be carried out using the appropriate mode. It may

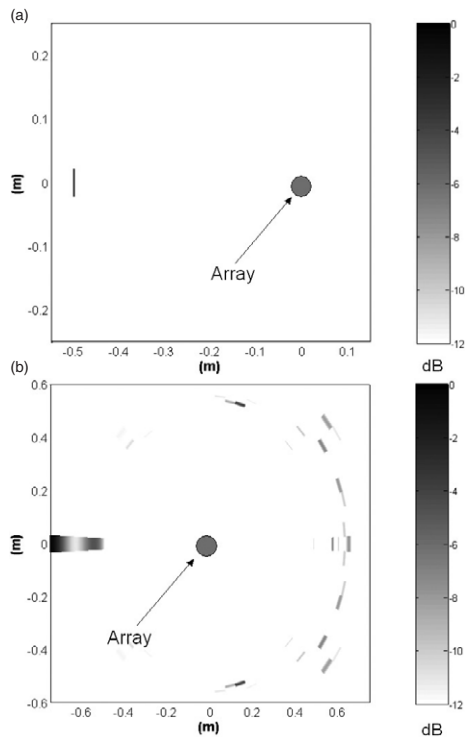


Figure 6. (a) Reconstruction, including dispersion, of a simulated defect 50 cm from the array center located along the 180° direction: excitation pulse at 2 MHz frequency. (b) Reconstruction of the case shown in figure 6(a), but ignoring dispersion.

be noted that defect location is ‘automatic’ in the angular domain by virtue of the phased addition reconstruction process. However, the radial position prediction is relative and requires a suitable scaling factor for determining the absolute positional information. This scaling factor could very well be provided by the edge of the structure or a rivet hole. Through the reconstruction of this standard structural feature, the algorithm can be calibrated to provide absolute positional information.

6. Experimental application

Three experiments, two using commercial transducers and one using a prototype STMR array, were performed. The first two experiments were to reconstruct the edges and a circular hole on an aluminum plate respectively, both using commercial PZT transducers. The third experiment again involved the reconstruction of the edges of an aluminum plate, but using the STMR array. The dimensions and thickness of the aluminum plates used in all three experiments were 60 cm × 60 cm and 1 mm respectively.

In the first experiment a Panametrics 5058PR Pulser/Receiver was used to excite a Panametrics Videoscanner 500 kHz transducer, which was used as a transmitter. A similar transducer was used as receiver. A 20 MHz Data Acquisition (DAQ) card was used for signal acquisition. The receiver was kept at 15 equi-spaced locations, one after another, on a circle of 8 cm diameter, with the transmitter at the center, and signals were obtained at each of these locations to simulate an array with 15 receivers. The transmitter was excited with a 100 V signal with center frequency of 500 kHz. The signals were

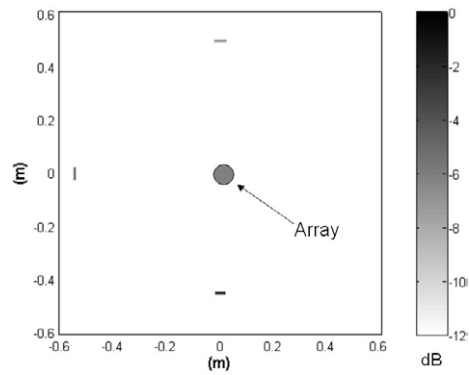


Figure 7. Reconstruction of three simulated defects 50, 55 and 45 cm from the array center located along the 90°, 180° and 270° directions respectively.

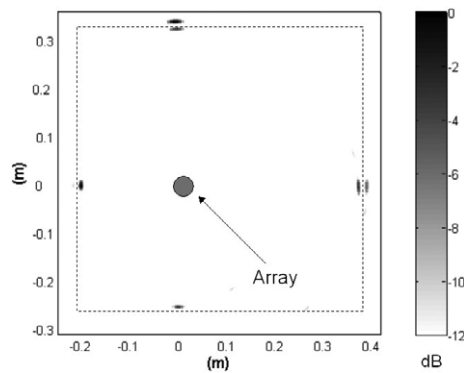


Figure 8. Reconstruction of edges of the aluminum plate with 12 dB range.

sampled at 2.5 MHz and filtered after acquisition using a band pass filter of 100–500 kHz range to eliminate high frequency noise and undesirable low frequency components. The S_0 mode was used for reconstruction since this was the fastest mode. In this experiment, the left, right, top, and bottom edges of the aluminum plate were 22, 38, 34 and 26 cm away from the array center (transmitter) respectively. Figure 8 shows the reconstruction with a 12 dB range with excellent sensitivity to the edges shown as dashed lines. The segments of the edges that are orthogonal to the wave front are most prominently imaged since the entire wave is reflected back to the array from them.

The second experiment, to reconstruct a circular hole, consisted of two stages. In the first stage reference signals from the defect-free plate were collected. In the second stage, the defect was introduced and the data were collected again. The defect-free data set was used to normalize the data obtained on the defective plate. This normalization was necessary to compensate for the reflections from the edges of the plate, which are substantially larger than the reflection from the defect. This procedure is similar to the actual structural health monitoring (SHM) process where the STMR array will most likely be used to obtain an initial baseline data after which it begins the process of monitoring the structure for detrimental structural damages.

For this experiment data acquisition was done using a different set of instrumentation in order to demonstrate that

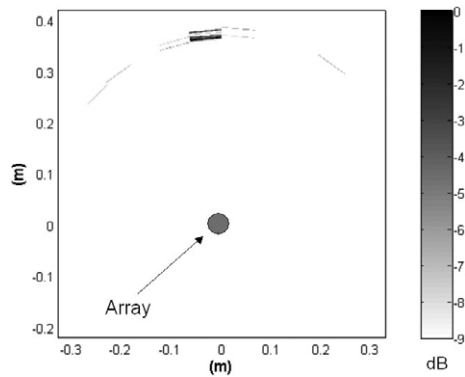


Figure 9. Reconstruction of the 7 mm circular hole.

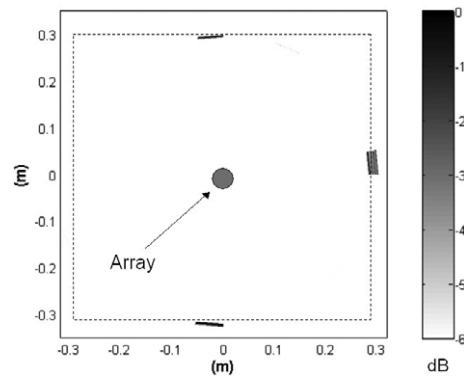


Figure 10. Reconstruction of the edges of a 60 cm \times 60 cm aluminum plate.

the technique can be adapted to different instrumentation. Instead of the Panametrics 5058PR Pulsar/Receiver a Matic Instruments PR5000 Pulsar/Receiver was used for exciting the transmitter, since higher gain settings were needed for imaging the defect. This, as mentioned before, was necessary because the reflection from a small defect is relatively very weak when compared to the edges that manifest as large defects. An Agilent 54621A oscilloscope was used instead of the DAQ card since it had the additional capability of averaging the signals, leading to a reduction in noise levels. Otherwise, the data acquisition process, the parameters for data acquisition and the mode used for reconstruction were the same as in the first experiment. In this experiment, the left, right, top, and bottom edges of the aluminum plate were 9, 51, 51 and 9 cm away from the array center respectively. The hole was located 38 cm away from the array center along the $\theta = 90^\circ$ direction. Figure 9 shows the imaging of the circular hole using the normalized data. As can be seen from the figure, the position of the reconstructed hole compares well with its actual location.

In the third experiment, the same instrumentation used in the second experiment was used. But unlike in the first two experiments, an STMR array (shown in figure 1) was used for signal acquisition. The STMR array, kept at the center of a 60 cm \times 60 cm aluminum plate, was used to obtain the reflected signals at all 15 locations simultaneously using a multiplex. The parameters used for signal acquisition of the mode used for reconstruction were the same as those used in the first two experiments. The reconstruction of the edges of the aluminum plate using the data obtained from this experiment is shown in figure 10 and compares well with figure 8.

7. Summary

In this paper, the feasibility of the structural health monitoring (SHM) of isotropic plate-like structures using an STMR array of PZT transducers has been demonstrated. Features and capabilities of the STMR system are as follows.

- (1) It requires a simpler electronics system with a reduced footprint, desirable for SHM of aerospace structures, when compared to other systems described in the literature.
- (2) It can handle dispersive effects of transmitted and received modes.
- (3) The use of a single transmitter as opposed to multiple transmitters prevents side lobe formation in the sent beam and avoids associated false alarms that these side lobes generate.
- (4) Deconvolution is not essential; although side lobes occur due to arraying of received signals, a simple thresholding provides for reasonable assessment of flaw detection and location.
- (5) It allows for improved angular resolution through the inclusion of a larger number of angles for reconstruction as well as by adjusting the diameter of the receiver ring, limited only by the physical sizes of the receivers.
- (6) It can work in single mode transmission—single mode reception, as well as in single mode transmission—partly mode converted reception.
- (7) It can in principle work even when the received mode is unknown, by allowing the algorithm to search through the various modes.
- (8) It permits reasonable positional accuracy for the flaw through calibration against a standard feature of the specimen such as an edge or a rivet hole.
- (9) It is tolerant to slight errors in the positioning of receivers and the transmitter with respect to each other.
- (10) Very light materials like PVDF film sensors (which have good reception capabilities but poor transduction capabilities) can be used as receivers in an STMR system along with a PZT transmitter. Other options include MEMS and fiber optics based sensor systems. This will result in a much lighter array system, which is critical for aerospace applications.
- (11) The PZT array shown here uses wires for transmitting data from the receivers. But with the rapid advances being made in RF MEMS technology, it is conceivable that this data transmission can be made wireless, leaving the transmitter alone to be wired. Also, the reduction in size of receivers will make it possible to accommodate more receivers and hence result in improved detection and imaging of flaws present in the structure.

The STMR system can also be designed to be self-calibrating by using the initial signal received by the receivers to measure the material properties that can then be used in the phase reconstruction algorithm. In order to use this algorithm

for more complex materials such as anisotropic and multi-layered fiber reinforced composites, the phase reconstruction algorithm must be modified, and this has been discussed elsewhere [5]. This technique is applicable to imaging features in the structure that reflect the guided waves back to one or more of the receivers. Hence, it can find applications where imaging of structural features such as edges, corners, and reinforcements, or the structural health monitoring of structures with such features, is anticipated.

Finally, for the work reported here, the STMR configuration was considered to be a circular array. However, other configurations such as semi-circular, elliptical, and rectangular arrays may be used, depending on the size and shape of the structure that is being monitored. The necessary changes in the algorithm can be made without any difficulty.

Acknowledgments

This work was funded by the Aeronautical Development Agency, Bangalore, through the DISMAS program.

References

- [1] Kessler S 2002 Piezoelectric based in-situ damage detection of composite materials for structural health monitoring systems *PhD Thesis* Massachusetts Institute of Technology, USA
- [2] Meeker T R and Meitzler A H 1964 Guided wave propagation in elongated cylinders and plates *Phys. Acoust. A* **1** 111–67
- [3] Alleyne D N and Cawley P 1992 The interaction of Lamb waves with defects *IEEE Trans. Ultrason. Ferroelectr. Freq. Control* **39** 381–97
- [4] Rose J L 1999 *Ultrasonic Waves in Solid Media* (Cambridge: Cambridge University Press)
- [5] Rajagopalan J, Balasubramaniam K and Krishnamurthy C V 2006 A phase reconstruction algorithm for Lamb wave based structural health monitoring of anisotropic multilayered composite plates *J. Acoust. Soc. Am.* **119** 872–8
- [6] Sicard R, Goyette J and Zellouf D 2002 A SAFT algorithm for lamb wave imaging of isotropic plate-like structures *Ultrasonics* **39** 487–94
- [7] Wilcox P D, Lowe M and Cawley P 2000 Lamb and SH wave transducer arrays for the inspection of large areas of thick plates *Rev. Prog. Quant. Non-Destruct. Eval. A* **19** 1049–56
- [8] Norton S J 2002 Synthetic aperture imaging with arrays of arbitrary shape-part I: general case *IEEE Trans. Ultrason. Ferroelectr. Freq. Control* **49** 399–403
- [9] Norton S J 2002 Synthetic aperture imaging with arrays of arbitrary shape-part II: The annular array *IEEE Trans. Ultrason. Ferroelectr. Freq. Control* **49** 404–8
- [10] Wilcox P D 2003 Omni-directional guided wave transducer arrays for the rapid inspection of large areas of plate structures *IEEE Trans. Ultrason. Ferroelectr. Freq. Control* **50** 699–709
- [11] Prasad S M, Balasubramaniam K and Krishnamurthy C V 2004 Structural health monitoring of composite structures using Lamb wave tomography *Smart Mater. Struct.* **13** N73–9
- [12] Prasad S M, Jagannathan R, Balasubramaniam K and Krishnamurthy C V 2004 Structural health monitoring of anisotropic layered composite plates using guided ultrasonic Lamb wave data *Rev. Prog. Quant. Non-Destruct. Eval.* **23** (B) 1460–7
- [13] Wilcox P D 2003 Guided wave beam steering from omni-directional transducer arrays *Rev. Prog. Quant. Non-Destruct. Eval.* **22** (A) 761–8
- [14] Sundararaman S, Adams D E and Rigas E J 2005 Structural damage identification in homogeneous and heterogeneous structures using beamforming *Struct. Health Monitoring* **4** 171–90
- [15] Wang C H, Rose J T and Chang F-K 2004 A synthetic time-reversal imaging method for structural health monitoring *Smart Mater. Struct.* **13** 415–23
- [16] Wilcox P D, Lowe M J S and Cawley P 2001 A signal processing technique to remove the effect of dispersion from guided wave signals *Rev. Prog. Quant. Non-Destruct. Eval.* **20** (A) 555–62